Directional solidification at high speed. I. Secondary instabilities

Klaus Kassner,[1] Chaouqi Misbah,[2,*] Heiner Müller-Krumbhaar,[1] and Alexandre Valance[2,*]
[1]*Institut für Festkörperforschung des Forschungszentrums Jülich, 52425 Jülich, Germany*
[2]*Institut Laue-Langevin, Boîte Postale 156, 38042 Grenoble Cedex 09, France*
(Received 11 November 1993; revised manuscript received 17 February 1994)

We present an extensive analytical and numerical analysis of secondary instabilities in directional solidification in the limit of high speed, which is by now accessible in real experiments. The important feature in this regime is that front dynamics are quasilocal. From symmetry and scaling arguments, we write down the general form of the nonlinear equation for the interface, an equation to which the present study pertains. In order to determine the values of the coefficients, a derivation from the fully nonlocal model was performed. We consider the general case where mass diffusion is allowed in both phases, and its special restrictions to the one-sided model (appropriate for regular materials), and the symmetric one (appropriate for liquid crystals). We first focus on the appearance of cellular structures (primary instability). In the symmetric case the structures are rather shallow, in accord with experiments. In the one-sided model, the front generically develops, in a certain region of parameter space, cusp singularities. These can be avoided by allowing a small amount of diffusion in the growing phase; the front then reaches a stationary state. Stationary states are in turn subject to instabilities (secondary instabilities). Besides the Eckhaus instability, we find parity-breaking (PB), vacillating-breathing (VB), and period-halving (PH) bifurcations, regardless of the details of the model, a fact which points to their genericity. Another line of research developed in this paper is the analytical analysis of these bifurcations. The PB and PH bifurcations are analyzed close to the codimension-two bifurcation point where the first and second harmonics are dangerous. The results emerging from this analysis are supported by the full numerics. The VB mode is analyzed analytically by means of an analogy with the problem of a quasi-free-electron in a crystal. Finally we discuss some questions beyond secondary instabilities. We find that this system exhibits an anomalous growth mode, observed in many systems. Among other pertinent features, we find that the broken-parity (BP) state is subject to a long-wavelength instability, causing a fragmentation of the extended state. This provides a signature of its "solitarylike" persistence observed in many experiments. Another important dynamical characteristic is that on increase of the growth speed the VB mode suffers a PB instability, and acquires a quasiperiodic motion (mixture of BP and VB modes which are incommensurate), which constitutes a prelude to a chaotic regime, discussed in the companion paper.

PACS number(s): 61.50.Cj, 81.30.Fb, 05.70.Fh

I. INTRODUCTION

When an impure solid is grown by directional solidification—that is, by pulling the sample at a constant speed along an external thermal gradient—the initially planar liquid-solid interface undergoes a morphological instability at a critical value of the pulling speed: the front turns into a periodic cellular structure on the scale of, say, a few μm. This is the Mullins-Sekerka [1] instability, driven by impurity diffusion. In general, the interface structure depends on three major factors: (i) the microscopic nature of the interface, i.e., whether it is smooth or rough; (ii) the amount of impurity diffusion in the growing phase; and (iii) the partition coefficient (that is, the ratio of the equilibrium impurity concentration in the solid to that in the liquid). Point (i) pertains to the roughening transition. Indeed, if the melting temperature is below the roughening one, the surface is microscopically smooth. The growth process operates basically through two-dimensional (2D) nucleation, and/or via screw dislocations. In such a case the surface shows faceted structures. This is a subject in which we are not interested here. Our study focuses on the other category, where the surface is rough on the microscopic scale. The resulting pattern is rounded. The importance of (ii) is that for ordinary materials, the diffusion coefficient in the solid phase is several orders of magnitude smaller than in the liquid phase; the diffusion is quasi-one-sided. In such a situation, the interface often develops deep grooves, which sometimes generate crystal defects, which—although very crucial for the quality of the solid—are rather secondary to the understanding of interface dynamics. The nematic system, experiments on which were first initiated by Oswald, Bechhoefer, and Libchaber [2], are canonical systems for the study of secondary instabilities—the primary instability denomination refers to that of the planar front. Indeed, there the impurity

*Present address: Laboratoire de Spectrométrie Physique, Université Joseph Fourier, 38402 Saint-Martin-d'Hères Cedex, France.

diffusion coefficients in both phases are of comparable orders of magnitude. This implies that the nematic system can support diffusion, whose main role is the creation of a short-circuit current which operates on the scale of a wavelength. As a consequence, the interface excursion remains limited; the structure is rather shallow. The importance of point (iii) is that a small partition coefficient implies more impurity accumulation in the grooves, thus reducing the growth dynamics there, and consequently increasing the front depletion.

The absence of deep grooves in this system makes it more flexible, in the sense that wavelength variation and adjustment are efficient on a time scale of the order of a second, while these are much longer with typical substances. This is one of the main reasons that makes the identification of secondary instabilities easier, and which has led to the discovery of many of them first in liquid crystals. As we shall see, most of the instabilities are common to both situations whether diffusion in the growing phase is negligible or not.

The denomination secondary instability is in general taken to mean that the cellular structure whose stability is investigated has bifurcated from a structureless state (the planar front). The instability from the planar front is referred to as the primary instability. However, this definition is somewhat restrictive. For example, the lamellar eutectic structure manifests instabilities similar to those we are investigating here, although that structure does not originate from the loss of stability of a planar interface; it originates from a complex transient mechanism, governed both by capillary forces—that enter the nucleation process—and interlamellar diffusion which is necessary for the cooperative growth of both solid phases. Therefore, we might find it useful to think of secondary instabilities as the instability of a cellular steady solution, regardless of the origin of that solution.

The problem of pattern formation has experienced an interesting revival since the discovery of various secondary instabilities that we shall describe below. Indeed, for a long time—basically since the Mullins-Sekerka work until a few years ago—the only secondary instability that was expected was the Eckhaus instability. The experimental effort by Simon, Bechhoefer, and Libchaber [3] on directional growth of a nematic phase gave the first evidence pertaining to what may be called the solitary mode. Indeed, it has been observed that at high enough growth speed, there appear small inclusions of asymmetric cells (a few cells), which have the following characteristics: they are approximately twice as wide as the symmetric cells, and they travel sideways at a constant speed. Since that discovery, similar observations have been made on different systems, such as eutectics [4], the printer system [5], and so on [6–8]. The fact that this mode of growth was observed in systems that seem diverse could point to the fact that it may be simply a disguised form of only a few prototypes. Coullet, Goldstein, and Gunaratne [9] suggested that this phenomenon may result from the loss of stability of the initially symmetric pattern. They built a phenomenological picture which contained some interesting features. It was shown later for eutectics [10] and for liquid-crystal systems [11] that the microscopic models do indeed support broken-parity (BP) solutions. The present instability is a parity-breaking (PB) one inasmuch as the original equations are symmetric under reflexion at the growth axis. We shall see that this instability always precedes a period-halving (PH) one.

Another secondary instability is the one which we have called vacillating breathing (VB), and for which we have already given a brief account [12]. This is an instability where the width of each cell oscillates in phase opposition with its neighbors; hence, this is a period-doubling instability.

Coullet and Ioos [13] use symmetry arguments to classify ten generic instabilities; those presented above are typical examples. It is important to know which of these instabilities can be realized within a specific system. Here we shall be concerned with an extensive study of secondary instabilities in directional growth. Since most of the instabilities observed on the nematic system occur at high enough speed, we shall concentrate on this situation. This regime offers a great advantage which lies in the (legitimate) possibility to reduce the original growth equations—which involve nonlocal and retarded interactions—to a rather simple quasilocal equation which is more tractable and on which we can easily exemplify many of our studies. We should keep in mind, however, that most of the reasoning (such as the explanation given for the VB mode) will work perfectly well with more complex equations. By using information from the dispersion relation for a planar front, we shall write the general form of the local equation by exploiting simple symmetry and scaling arguments. In order to find the coefficients of that equation, one needs, of course, to perform the derivation of the evolution equation from the constitutive equations. In order to check that our results are not specific to liquid-crystal systems, we shall study the dynamics in the general situation where allowance of an arbitrary diffusivity in the growing phase is made. We find that the evolution equation accounts for (i) the Eckhaus instability, (ii) a period-halving bifurcation, (iii) parity breaking, and (iv) vacillating-breathing, regardless of the details of the model. The first instability is by now classical, and we shall be brief in discussing it.

This equation also manifests other features that go beyond secondary instabilities. A question that remains to be elucidated pertains to the stability of the broken-parity (BP) mode as an extended state. It emerges here that this mode suffers a long-wavelength instability, which we believe is caused by the persistence of the Eckhaus instability. The BP state undergoes a fragmentation process, which is a signature of its solitary character, reported on in many experiments. Another important result is the coexistence of the BP and VB modes, a coexistence which is persistent in many experimental situations. These two modes seem often to maintain their identity; the motion is quasiperiodic. A relatively small variation of the growth velocity is sufficient to lead to chaos via a quasiperiodic scenario. The transition to chaos is the subject of the companion paper.

We should stress the fact that although this paper and its companion deal with a variety of static and dynamical

features, they are far from exhausting all possible scenarios. For example, at high speed there are some experiments which manifest rich dynamics, such as banded structures, which may require the inclusion of additional ingredients, namely kinetic effects [14]. Our main message is that all the features encountered here (going from order to chaos, and possibly other dynamics not studied here) are accounted for within the minimal version of crystal growth.

The scheme of this paper is as follows. In Sec. II we set down the growth equation, and recall the Mullins-Sekerka dispersion relation in the general case of the two-sided model. In Sec. III we concentrate on the large speed limit. We determine the characteristic time and space scales. Then, using symmetry and scaling arguments, we set down the general form of the evolution equation. In Sec. IV, we give the evolution equation obtained from the microscopic model. In Sec. V we proceed to the determination of the steady-state solutions, and their range of existence for liquid crystal systems, and then study secondary instabilities. In Sec. VI, we discuss the same problem as in Sec. V for ordinary materials. Section VII is devoted to the analytical analysis of secondary instabilities. Section VIII presents some results that go beyond secondary instabilities. Section IX sums up our results.

II. BASIC EQUATIONS

A binary system is pulled at constant speed V along the $-z$ direction, parallel to a thermal gradient G. As usual we neglect heat transport, and assume that the thermal properties of both phases are identical. The minimum version of crystal growth is by now standard, so we shall directly write down the basic equations. Let c and c' denote the concentrations (defined as the number per unit mass) of the minor component of the alloy in the solid (or nematic) and liquid phases, respectively. We introduce the dimensionless fields $u=(c-c_\infty)/\Delta c$ and $u'=(c'-c_\infty)/\Delta c$ in both phases, where c_∞ is the initial liquid concentration, $\Delta c=c_\infty(1-k)/k$ is the equilibrium miscibility gap, where k is the partition coefficient. Lengths and time will be measured in units of $l=2D/V$ and l^2/D, where V is the pulling speed, and D is the diffusion constant in the liquid phase. In the bulk phases u and u' obey mass conservation laws:

$$\frac{\partial u}{\partial t}=\nabla^2 u+2\frac{\partial u}{\partial z}\ ,\quad z>\zeta(x,t)\ , \tag{2.1}$$

$$\frac{\partial u'}{\partial t}=\nu\nabla^2 u'+2\frac{\partial u'}{\partial z}\ ,\quad z<\zeta(x,t)\ , \tag{2.2}$$

where $\zeta(x,t)$ is the instantaneous front position (we consider only $1D$ deformations), and $\nu=D'/D$. For the one-sided model, $\nu=0$, while $\nu=1$ for the symmetric model. Since the concentration far ahead of the advancing front is maintained at $c=c_\infty$, we have $u(z\to\infty)=u'(z\to-\infty)=0$. The concentration fields are subject to the continuity equation at the front $[z=\zeta(x,t)]$:

$$\nu\frac{\partial u'}{\partial n}-\frac{\partial u}{\partial n}=(2+\dot\zeta)n_z[k+(1-k)u]\ , \tag{2.3}$$

where $\partial/\partial n$ stands for the normal derivative, and n_z is the z component of the normal which is taken to point from the solid into the liquid. In Eq. (2.3) we have made use of the condition $c'=kc$ at the front, which amounts in reduced variables to

$$u'=k(u-1)\ . \tag{2.4}$$

Finally chemical equilibrium at the front (appropriate for molecularly rough interfaces) implies

$$u=1-\frac{\zeta}{l_T}-d_0\kappa\ , \tag{2.5}$$

where

$$d_0=\frac{\gamma T_M}{mlL\Delta c}\ ,\quad l_T=\frac{m\Delta c}{lG} \tag{2.6}$$

are the reduced (by l) capillary and thermal lengths respectively, where γ is the surface tension, T_M the melting temperature of the pure substance, m the absolute value of the liquidus slope, L the latent heat per unit volume, and κ the front curvature taken to be positive for a convex profile

$$\kappa=-\frac{\zeta_{xx}}{(1+\zeta_x^2)^{3/2}}\ , \tag{2.7}$$

where here and in future differentiations are subscripted. The set of Eqs. (2.2)–(2.5) completely describes the growth dynamics. This set admits a steady-state planar solution moving at speed V, the linear stability analysis of which yields the following dispersion relation [15]:

$$\omega+2-\omega_q(1-k)-(2-\omega_q)\sqrt{1+q^2+\omega}+k\omega_q\sqrt{1+\nu^2q^2+\nu\omega}=0\ , \tag{2.8}$$

where ω is the amplification (or attenuation) rate, q the wave number of the perturbation, and $\omega_q\equiv d_0q^2+l_T^{-1}$. The planar front is stable if $\mathrm{Re}(\omega)<0$ for all q's. Conversely, it is unstable if $\mathrm{Re}(\omega)>0$ at least for one particular value of q. The critical situation is attained when $\mathrm{Re}(\omega)=0$ for a particular value of q, say q_c, while $\mathrm{Re}(\omega)<0$ for all other q's. It can be shown [15] that if $\mathrm{Re}(\omega)=0$, then $\mathrm{Im}(\omega)=0$, that is to say the Mullins-Sekerka instability is steady. So, when studying the bifurcation we can simply set $\omega=0$ in (2.8). The resulting equation relates the wave number q to the control parameters (e.g., V and G). The associated curve (the neutral curve) is shown in the diagram (q,V) in Fig. 1. The neutral curve is a tongue: at small V the planar front bifurcates into a cellular state at $V=V_1$ (see Fig. 1), and it bifurcates back to a planar front at $V=V_2$ (the origin of this restabilization is that at high speed the capillary length becomes comparable to the diffusion length). In this paper we are mainly interested in the high velocity regime, or equivalently in the large Péclet number limit (defined by $P=\lambda V/D$). For example, in Fig. 1, even at $V/D=30\simeq 6V_1$, the Péclet number inside the unstable domain goes approximately from 1 to 11 (at the linearly most dangerous line—the dashed line—it is on the order of 2). These are large Péclet numbers. Since the cells in-

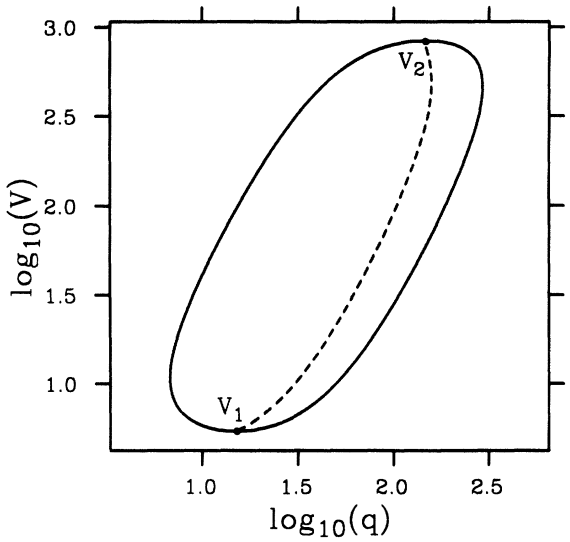

FIG. 1. The tongue in the velocity-wave-number plane inside which the planar front solution is unstable. V_1 is the lowest value for the instability, while V_2 corresponds to the critical value for restabilization. Parameters: $d_0=10^{-3}$, $l_T=0.5$, $D=D'=1.0$, and $k=1.0$. The dashed line indicates the position of the most unstable mode.

teraction via the diffusion field decays exponentially with the distance, the above Péclet numbers lead to localized interactions. In Sec. III we shall give from scaling and symmetry arguments the general form of the local equation. Although our treatment can be made more general than what is presented below, we shall concentrate on the situation close to the absolute stability limit. Thanks to the large values of the Péclet number mentioned above, we expect the asymptotic analysis to accurately describe the dynamics even far away from the absolute stability limit.

III. LOCAL EVOLUTION EQUATION

In this section we shall first give the general evolution equation from symmetry and scaling arguments. The starting point is the determination of the characteristic temporal and spatial scales of the dynamics. This is done by analyzing the dispersion relation (2.8). In order not to complicate the explanation of the strategy unnecessarily, we shall first consider the symmetric case, with a constant miscibility gap [that is, we set $\nu=1$ and $k=1$ in Eq. (2.8)]. The resulting dispersion relation then takes a simpler form

$$\omega+2=2(1-l_T^{-1}-d_0q^2)(1+q^2+\omega)^{1/2} . \tag{3.1}$$

The bifurcation is defined by $\omega=0$ and $\partial\omega/\partial q=0$ (it is represented by the two extrema in Fig. 1, and we are interested in the dynamics close to the upper maximum). These two conditions provide

$$1-l_T^{-1}=3\left[\frac{d_0}{4}\right]^{1/3}-d_0 , \tag{3.2}$$

$$q_c^2=\left[\frac{1}{4d_0^2}\right]^{1/3}-1 . \tag{3.3}$$

These two relations determine the critical conditions for the onset of instability, and the critical wave number. Equation (3.3) is meaningful only if $d_0\leq\frac{1}{2}$. In the limit $d_0\to\frac{1}{2}$ we have $q_c\to 0$. We concentrate on the extreme limit where $d_0\to\frac{1}{2}$ (at that limit the Péclet number goes to very large values). It is useful to introduce a small parameter

$$\epsilon=\tfrac{1}{2}-d_0 , \tag{3.4}$$

which measures the distance from the threshold, but in reality it can be thought of as the inverse of the Péclet number. It follows from Eq. (3.3) that q_c scales as

$$q_c^2=\tfrac{4}{3}\epsilon+\text{h.o.t.} \tag{3.5}$$

while Eq. (3.2) provides

$$l_T^{-1}=\tfrac{2}{3}\epsilon^2+\text{h.o.t.} , \tag{3.6}$$

where h.o.t. stands for higher-order terms. Equation (3.5) shows that the dynamics are described by long-wavelength modes (in comparison to the diffusion length). According to the scaling in Eqs. (3.5) and (3.6), it is appropriate to introduce quantities of order unity $\bar{q}$ and $\bar{l}_T^{-1}$ defined by $q=\sqrt{\epsilon}\bar{q}$ and $l_T^{-1}=\bar{l}_T^{-1}\epsilon^2$. Then using both these definitions with that of ϵ, we obtain from Eq. (2.8) that $\omega\sim\epsilon$, so that the dispersion relation takes the following form:

$$\epsilon^2[\bar{\omega}^2+4\bar{q}^2\bar{\omega}+8\bar{l}_T^{-1}+3\bar{q}^4-8\bar{q}^2]+\text{h.o.t.}=0 , \tag{3.7}$$

where $\bar{\omega}=\omega/\epsilon$. In real space, Eq. (3.7) provides

$$\epsilon^2[\zeta_{TT}-4\zeta_{XXT}+3\zeta_{XXXX}+8\zeta_{XX}+8\bar{l}_T^{-1}\zeta]+\text{h.o.t.}=0 . \tag{3.8}$$

Since the Fourier variables $\bar{q}$ and $\bar{\omega}$ are scaled by $\epsilon^{-1/2}$ and ϵ^{-1}, we have accordingly introduced slow variables X and T related to the original variables x and t by

$$X=x\sqrt{\epsilon} , \quad T=\epsilon t . \tag{3.9}$$

At small ϵ the linear contribution in Eq. (3.8) becomes small enough so that nonlinear terms become more and more relevant. Now the question is which type of nonlinear terms are to enter the dynamics, without resorting to calculation from the microscopic model. These terms can be obtained from a combination of symmetry and scaling arguments. Let us first consider quadratic nonlinearities. Because of the parity symmetry only even derivatives in x should appear. On the other hand, the only term that breaks the translational symmetry along the z direction is the one associated with the thermal gradient. Since it is linear in ζ it has already been accounted for in the linear part of the equation [Eq. (3.8)]. Therefore all the nonlinear terms to appear below are necessarily derivatives of x. Let us begin with those terms where only spatial derivatives are present. We have both quadratic and cubic terms. Consider first the quadratic terms.

(i) Quadratic nonlinearities

The most general quadratic term compatible with symmetries is of the form

$$\zeta_x{}^n\zeta_x{}^m , \quad n+m=4 . \tag{3.10}$$

The requirement that $n+m=4$ follows from the fact that since x scales as $\epsilon^{-1/2}$; this is the only way to obtain ϵ^2 as a contribution, and thus to balance the linear terms in (3.8). Since linear terms are already accounted for, we consider only the case where $n, m>0$. The only possibilities for $n=1$ and $m=3$ (and vice versa) and $n=2$ and $m=2$, so that the terms sought are

$$\zeta_x\zeta_{xxx} , \quad \zeta_{xx}^2 . \tag{3.11}$$

(ii) Cubic nonlinearities

The most general cubic nonlinearity takes the form

$$\zeta_x{}^m\zeta_x{}^n\zeta_x{}^p , \quad n+m+p=4 . \tag{3.12}$$

Here we have only one distinguishable case (that respects symmetry), namely $m=1$, $n=1$, and $p=2$ (and a circular permutation which produces similar terms). Thus we have as a cubic term of the form

$$\zeta_x^2\zeta_{xx} . \tag{3.13}$$

There are also terms where both derivatives of x and t can be present which are allowed by both scaling and symmetry. Consider separately quadratic and cubic terms.

(i) Quadratic nonlinearities

$$\zeta_x{}^m\zeta_t{}^n{}_x{}^p , \quad m+p+2n=4 , \tag{3.14}$$

where we have made use of the fact that t scales as ϵ^{-1}. Requiring $m\neq 0$ (nonlinearity) and $n\neq 0$ (presence of a time derivative), we find that $n=1$, and hence $m+p=2$. So in total we have the following terms:

$$\zeta_{xx}\zeta_t , \quad \zeta_x\zeta_{xt}=\tfrac{1}{2}(\zeta_x^2)_t . \tag{3.15}$$

(ii) Cubic nonlinearities

The most general term is of the form

$$\zeta_x{}^n\zeta_x{}^m\zeta_t{}^p , \quad m+n+2p=4 . \tag{3.16}$$

The only possibility is $m=n=p=1$,

$$\zeta_x^2\zeta_t . \tag{3.17}$$

Finally there are fourth-order terms, compatible with the scaling and the parity symmetry. It can easily be checked that there is one term, which is

$$\zeta_x^4 . \tag{3.18}$$

It is clear that higher-order nonlinearities produce terms with ϵ^n with $n>2$, and therefore should not be retained. The full nonlinear equation is the collection of the above terms [Eqs. (3.11), (3.13), (3.15), (3.17), and (3.18)], added to the linear equation (3.8), which we shall write by using the slow variable X and T:

$$\begin{aligned}\zeta_{TT}-4\zeta_{XXT}+3\zeta_{XXXX}+8\zeta_{XX}+8\bar{l}_T^{-1}\zeta \\ =\alpha_1\zeta_{XX}^2+\alpha_2\zeta_X\zeta_{XXX}+\alpha_3\zeta_X^2\zeta_{XX}+\alpha_4\zeta_T\zeta_{XX} \\ +\alpha_5\zeta_X\zeta_{XT}+\alpha_6\zeta_X^2\zeta_T+\alpha_7\zeta_X^4 ,\end{aligned} \tag{3.19}$$

where the α_i's are real coefficients. In order to determine these coefficients we need to calculate them from the microscopic model under consideration, while the general form of Eq. (3.19) follows from symmetry and scaling arguments [16].

In reality, we have not yet exploited all the symmetries. The only symmetries which we have hitherto evoked are the reflection symmetry and translational symmetries. There is, however, another symmetry group which needs to be considered: the full rotational symmetry. This symmetry is more manifest when we use intrinsic coordinates. Indeed, besides the gauge-invariant formulation of the evolution of the geometry (i.e., the curvature evolution) the normal velocity (which is the physical component of the front velocity) contains the curvature and its covariant derivatives only, due to rotational symmetry. It can be shown [16] that when exploiting this symmetry, the coefficients $\alpha_6=0$ and $\alpha_7=0$ in Eq. (3.19).

IV. EVOLUTION EQUATION IN THE TWO-SIDED MODEL

There have been derivations of the evolution equation in the two limits of the one-sided [17] and symmetric models [18]. The strategy for the deviation in the two-sided model is similar [19], and we shall directly give the result and comment upon it briefly,

$$\begin{aligned}\zeta_{TT}-\left[2+\frac{1}{k}+\nu\right]\zeta_{XXT}+\left[1+\frac{1}{k}+\nu^2\right]\zeta_{XXXX}+8k\zeta_{XX}+8kl_T^{-1}\zeta \\ =2\zeta_T\zeta_{XX}+2(\zeta_X^2)_T-2(\zeta_X^2)_{XX}-2\nu\zeta_X\zeta_{XXX}-\frac{2}{k}(\zeta_{XX}\zeta_X)_X-2[(\zeta_X)^3]_X .\end{aligned} \tag{4.1}$$

A simple inspection of this equation shows that only the terms that were derived from symmetry and scaling [Eq. (3.19)] are present (one may need to perform some differentiations in the above equation to check this point).

The above equation reduces to the one for the one-sided model [17] for $\nu=0$ and to the symmetric one with a constant miscibility gap for $\nu=1$ and $k=1$ [18]. Note that for the stationary problem, the one-sided model equation obviously possesses a first integral, and that therefore the mean front position is zero, while the mean

position in the two-sided case is positive. Both are consequences of mass conservation on the global scale.

V. FRONT DYNAMICS FOR LIQUID CRYSTALS

The symmetric model with a constant miscibility gap is appropriate for the liquid-crystal system. We shall characterize the steady pattern below, then proceed to a search for secondary instabilities.

A. Steady-state and symmetric solutions

In the limit of symmetric diffusion with a constant miscibility gap ($v=1, k=1$), the steady-state version of Eq. (4.1) takes the form

$$3\zeta_{0XXXX}+8\zeta_{0XX}+8l_T^{-1}\zeta_0 = -4(\zeta_{0X}^2)_{XX}-2(\zeta_{0X}^3)_X+2\zeta_{0XX}^2 \ . \quad (5.1)$$

We consider periodic solutions with a wavelength λ. Moreover, we restrict ourselves to symmetric solutions. Equation (5.1) is a nonlinear equation for the unknown ζ_0, and is of fourth order in space, thus requiring four boundary conditions. These are obtained from the requirement that $\zeta_{0X}=0$ and $\zeta_{0XXX}=0$ at the two ends of the interval, which we take as $[0, \lambda/2]$. This means that Eq. (5.1) admits, in principle, arbitrary solutions parametrized by the wavelength λ. We have solved this equation by means of a shooting method. Our results are summarized in Fig. 2. in the plane (l_T^{-1}, q) where the solid line represents the neutral curve for the stability of the plane front solution. Solutions exist inside the domain where the plane front solution is unstable. Their range of existence is delimited by the triangles. They extend up to the neutral curve for large wave number, and cease to exist for small-wave-number solutions with q as a basic wave number, whereas solutions with a basic wave number $2q$ merge. In other words, the basic solution undergoes tip splitting. This phenomenon is associated, as we shall see in Sec. VII, with a strong resonance between the first and second harmonics.

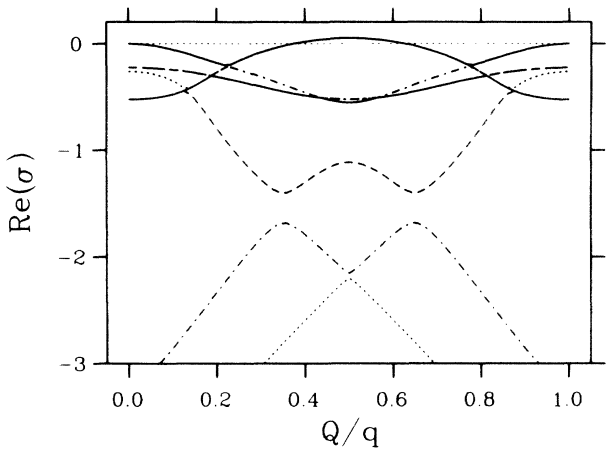

FIG. 3. An example of the stability spectrum following from the Floquet-Bloch analysis. Here $l_T^{-1}=0.28$ and $q=0.9$. There is an oscillatory instability at $Q=q/2$ (see text, Sec. V D).

The determination of steady-state solutions is a first step in the analysis of any pattern-forming system. The next natural step is to investigate their stability. The stability analysis has been presented elsewhere [12,19]. We just give the results here, based on a Floquet-Bloch analysis of the stability matrix. Figure 3 gives an example for the real part of this spectrum. Note that there is (always) a mode with a zero eigenvalue corresponding to translations of the pattern along the x direction. All patterns are only marginally stable with respect to that mode.

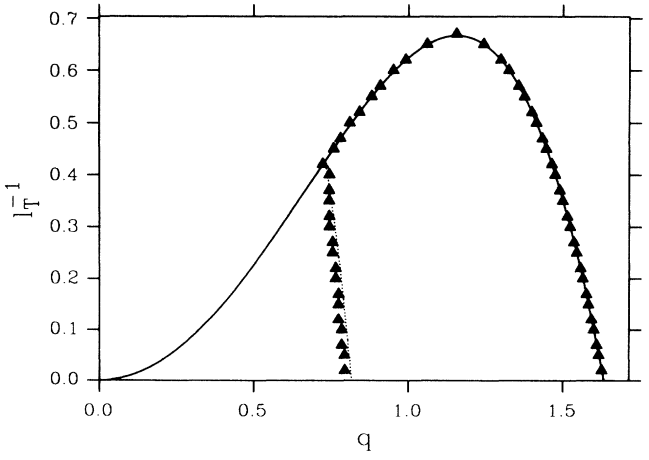

FIG. 2. The triangles delimit the region of existence of steady and symmetric solutions. Note that for small enough q (approximately when the mode $2q$ becomes neutral, which happens at the dotted line) the q family ceases to exist, bifurcating into a $2q$ family.

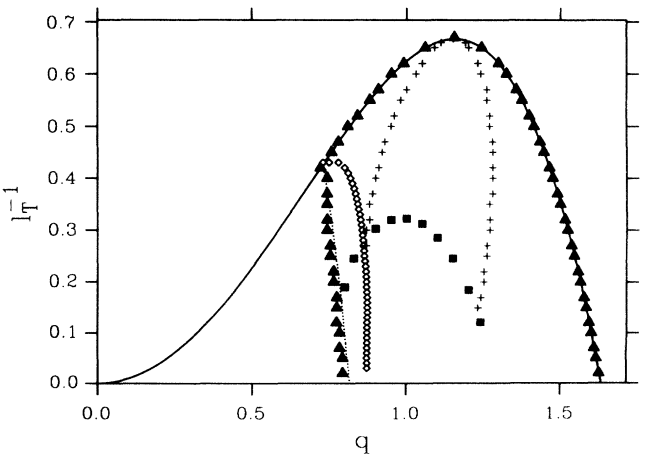

FIG. 4. Stability diagram in the plane l_T^{-1} vs q. Full line: the neutral curve; triangles: the limit of existence of steady solutions; crosses: the Eckhaus boundary; (open) diamonds: the boundary to the left of which broken-parity solutions appear; and (filled) squares: the boundary below which the VB mode appears.

B. Eckhaus instability

The first and, by now, classical instability is the Eckhaus instability. This is the most generic instability which occurs in many systems. The reason is traced back to symmetry. Indeed for an extended system there is a Goldstone mode, to which the pattern is indifferent, corresponding to a constant shift of the pattern along X. The phase is a conjugate variable to the Goldstone mode, and is therefore a dangerous mode. We can proceed to the investigation of phase instability by using the phase dynamics techniques [20,21]. We shall not follow this spirit here, but rather phase instability will follow from our stability analysis. The idea is to vary q within the domain of existence of steady solutions until we find a first positive eigenvalue. We find a wave-number domain (delimited by the crosses in Fig. 4) where one eigenvalue goes from negative to positive when crossing that domain outward. All the other branches have a negative real part. The most dangerous branch is represented in Fig. 5 below and above the instability threshold. This instability appears first at the origin of the Brillouin zone. It is purely real when $\mathrm{Re}(\sigma)>0$, and it behaves like $\sigma \sim Q^2$ at small Q. This is a purely diffusive instability. The analysis of the associated eigenmode shows indeed that this is a phase mode. The Eckhaus instability is of long-wavelength type. Figure 6 shows the dynamical solution (the numerical method is described in the companion paper) of the full Eq. (4.1). There we show the manifestation of the Eckhaus instability. We first force the wave number inside the Eckhaus-unstable domain (outside the crosses in Fig. 4) and take the steady solution as an initial structure. In order to allow for the manifestation of such an instability, the computational box should be taken large enough (more than five basic wavelengths). The figure shows the transient where the instability appears as a long-wavelength modulation of the periodicity, which leads (in the present case) to the creation of an additional cell; the subsequent adjustment operates via a phase diffusion process. The pattern has increased its wave number; the final wave-number is inside the Eckhaus-stable region.

C. Parity breaking

For values of l_T^{-1} not too far from the critical one, the only instability is the Eckhaus one. When l_T^{-1} is decreased the second harmonic becomes more and more competitive, especially in the small-wave-number range. There a new instability appears exactly at the center of the Brillouin zone ($Q=0$). The diamonds in Fig. 4 represent the boundary to the left of which this instability

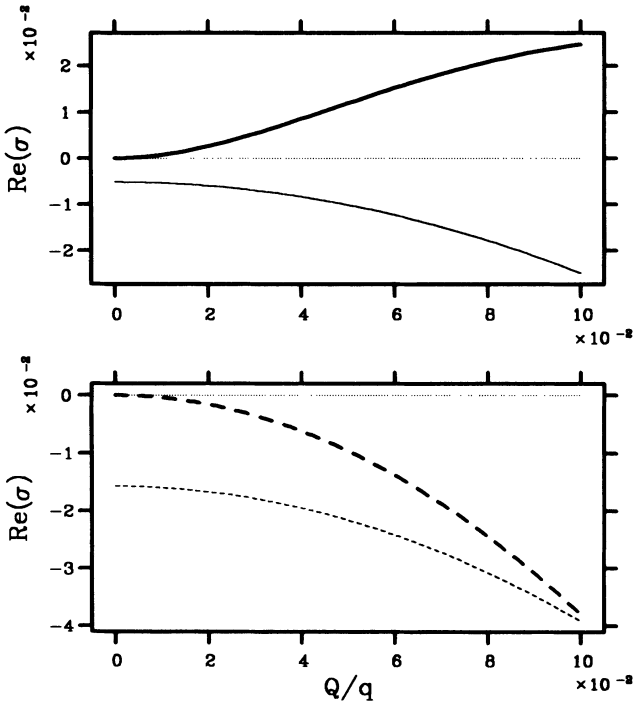

FIG. 5. The spectrum associated with the Eckhaus instability. Only the two most dangerous eigenvalues are shown. Top (solid lines): an unstable case ($l_T^{-1}=0.6$ and $q=1.0$); bottom (dashed lines): a stable situation ($l_T^{-1}=0.6$ and $q=1.1$). The imaginary part of the least stable mode is zero in both cases.

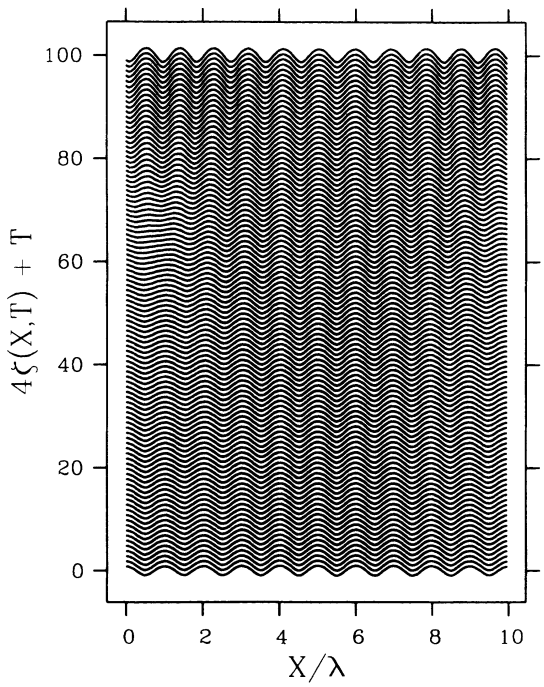

FIG. 6. Dynamical manifestation of the Eckhaus instability. In this and all following space-time portraits, the y axis is a hybrid space-time coordinate. Unless stated otherwise, the units correspond to the nondimensional space and time units defined by the scalings explained in the text. The x axis corresponds to the spatial extension of the pattern. Its unit is the wavelength of the basic symmetric solution. In this particular example, the height of the cells has been multiplied by four for better visibility. Here, $l_T^{-1}=0.6$ and $q=1.0$. The initial wave number is inside the Eckhaus-unstable band. The front undergoes tip splitting before it reaches a final wave number $q=1.1$ inside the Eckhaus-stable band.

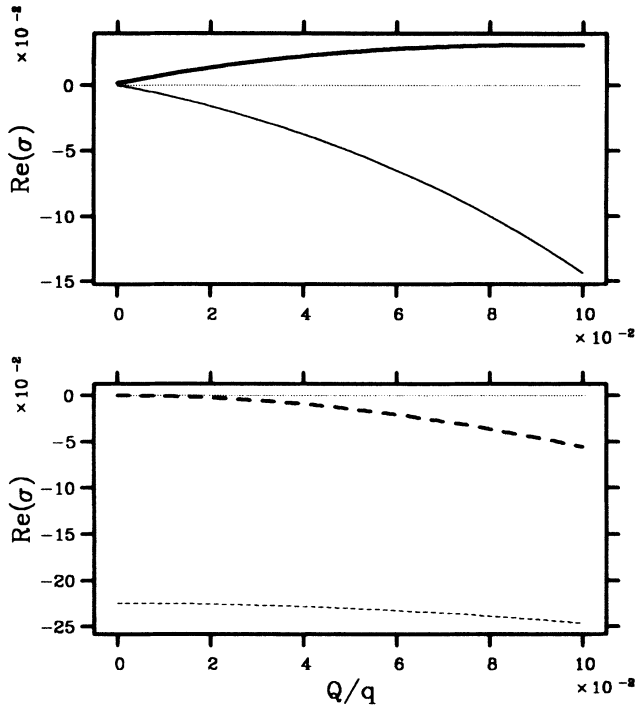

FIG. 7. The spectrum which corresponds to the PB instability. This instability is at $Q=0$. Shown are the two eigenvalues with the largest real parts. Top (solid lines): unstable case $-l_T^{-1}=0.28$ and $q=0.86$; bottom (dashed lines): stable case $-l_T^{-1}=0.28$ and $q=0.9$. The imaginary part of the upper branch is zero.

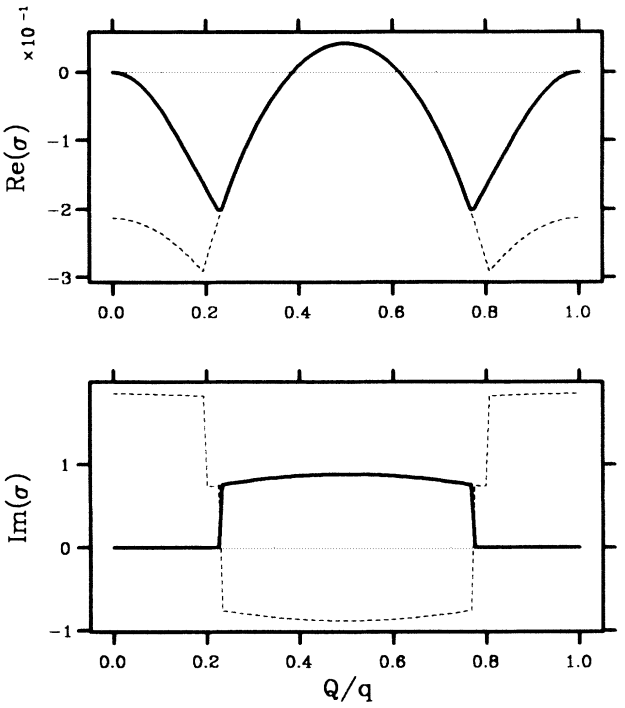

FIG. 9. The spectrum which corresponds to the VB instability. Top: the real part of the first two eigenvalues; bottom: the imaginary part. This instability occurs at $Q=q/2$, and is oscillatory.

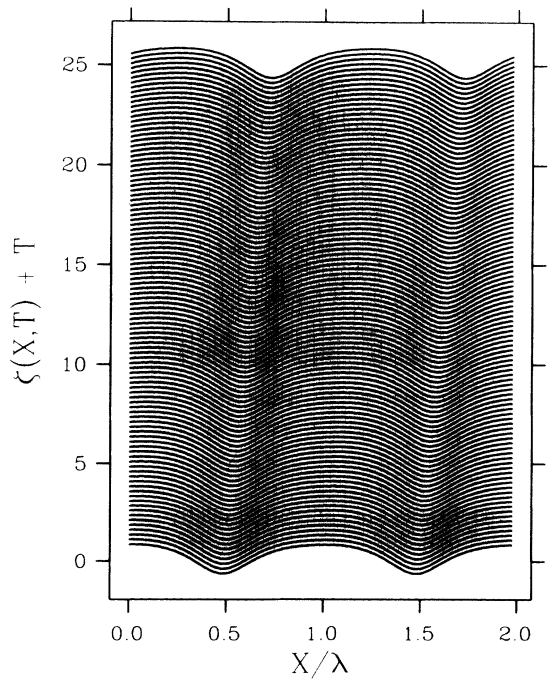

FIG. 8. The spatiotemporal portrait of the BP state, for $l_T^{-1}=0.28$, $q=0.86$. Because this is a situation very close to the stability threshold, the cells are almost symmetric and the drift velocity is small. For a faster drifting pattern, see Fig. 12.

occurs, while Fig. 7 shows the spectra below and above the instability. The analysis of the associated eigenmode shows that this instability is led by antisymmetric fluctuations. The numerical solution of the full Eq. (4.1) above the instability threshold shows the evolution of the pattern after transients have decayed (Fig. 8). The pattern is

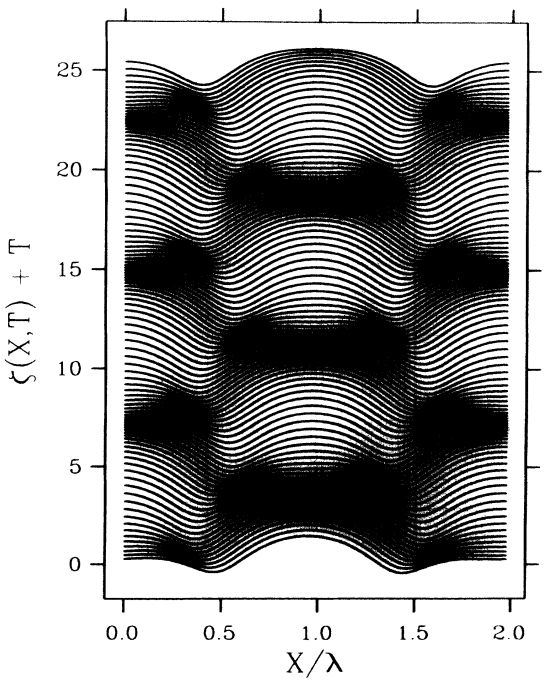

FIG. 10. The spatiotemporal portrait for the VB mode, where $l_T^{-1}=0.285$ and $q=0.9$.

asymmetric with respect to the growth axis, and travels sideways at a constant speed. In Sec. VII we discuss the analytic result for parity-breaking.

D. Vacillating breathing

We have discovered another instability. This appears below the curve given by the solid squares in Fig. 4. This instability occurs exactly at the boundary of the Brillouin zone ($Q/q=\frac{1}{2}$), and is oscillatory. Figure 9 shows the real and imaginary parts of the spectrum. This is a *period-doubling* instability very similar to the Peierls instability in one-dimensional conductors. The main difference is the oscillatory behavior, related to the nonadjoint character of the linear operator in the present case. In Sec. VII we shall return to an analytical analysis of this instability. The full numerical solution above the instability threshold is shown in Fig. 10. There we see that each cell oscillates in phase opposition to its neighbors (vacillation), while the top of each cell vibrates in a breathing fashion.

VI. FRONT DYNAMICS IN ORDINARY MATERIALS

The results presented in Sec. V refer to the liquid-crystal system, where mass diffusion is quasisymmetric. The question naturally arises of whether or not the above phenomena would persist in more general situations. In ordinary materials the mass diffusion coefficient in the solid phase is several orders of magnitude smaller than in the liquid phase. In the extreme limit of the one-sided model we found that at a large enough distance from the instability threshold, the interface develops cusp singularities at finite time (Fig. 11), and no steady solution is found. However, if a small amount of mass diffusion is allowed (approximately $\nu=0.01$) in the solid phase, this problem is cured. That is to say that stationary solutions are reached. Here we find the same scenarios as in liquid-crystal systems. Therefore we shall not linger on details, but rather directly give the overall picture of our findings. Figure 12 shows the broken-parity state, and Fig. 13 the vacillating-breathing mode. The main difference in comparison with the liquid-crystal system (Fig. 10) is the larger depth of the grooves between the cells, which makes the picture more impressive by emphasizing the vacillating motion. Although this cannot be inferred from the picture, one expects that in a system rescaled to physical variables the vacillating-breathing motion is much less pronounced in the one-sided case than in liquid-crystal systems. The reason is that the VB

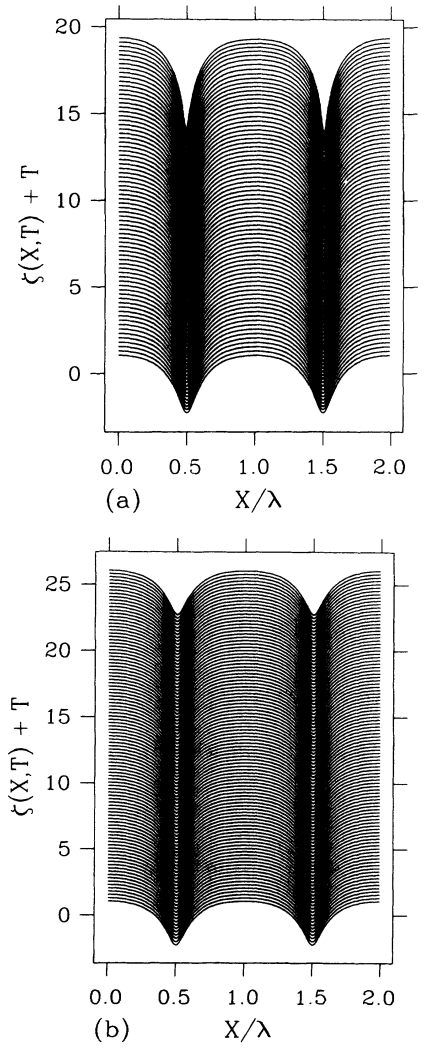

FIG. 11. A pattern showing the development of a cusp singularity (a) in the one-sided model ($\nu=0$), which is cured after allowance of a small amount of diffusion ($\nu=10^{-2}$) in the solid phase (b). Parameters: $l_T^{-1}=0.5$ and $q=1.2$.

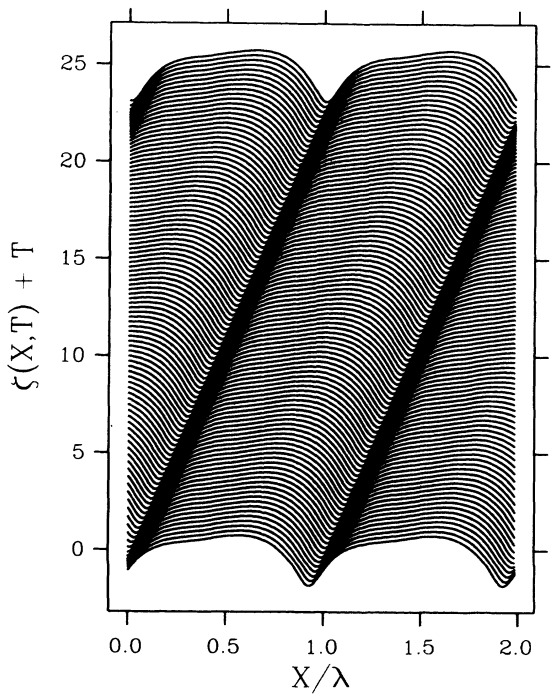

FIG. 12. The spatiotemporal portrait of a BP state in the one-sided model ($\nu=0$). Parameters: $l_T^{-1}=0.55$ and $q=1.0$.

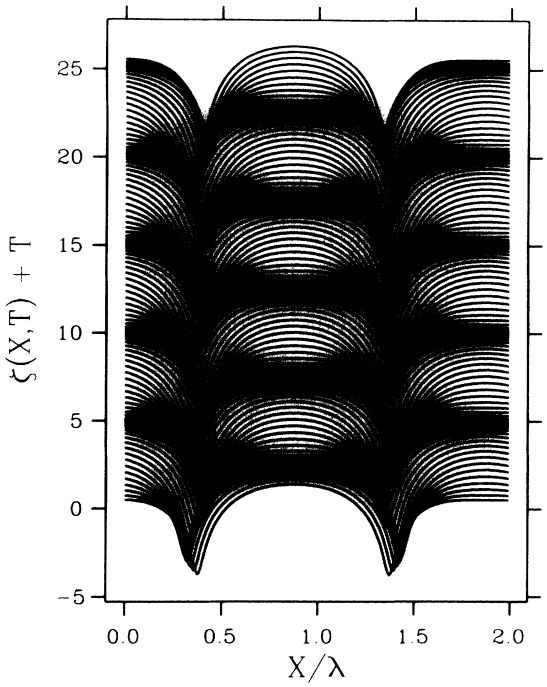

FIG. 13. The spatiotemporal portrait of the VB state in the one-sided model. Parameters: $l_T^{-1}=0.52$ and $q=1.2$.

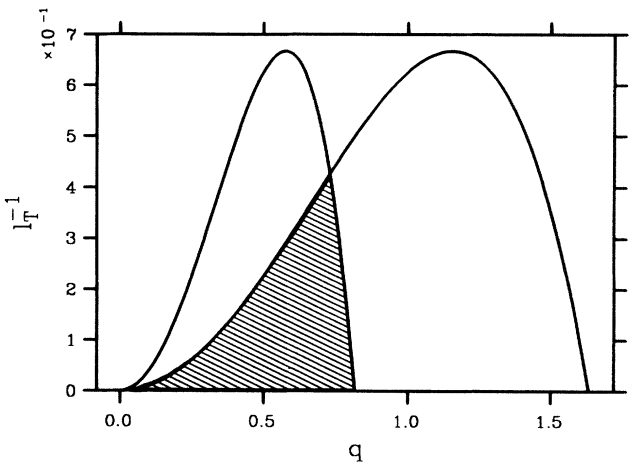

FIG. 14. The neutral curves $\omega(q)=0$ and $\omega(2q)=0$ in the plane l_T^{-1} vs q. The hatched region corresponds to the situation where both the q and $2q$ harmonics are unstable. The intersection point is the codimension-two point where the two harmonics bifurcate simultaneously.

mode implies an oscillatory melting-recrystallization process. In the quasi-one-sided model, the melting process is drastically reduced, since mass diffuses in a much slower manner in the solid phase, a fact which acts against the amplification of this mode. This is the main reason that this type of mode was first discovered in liquid crystals, but now its experimental evidence in ordinary materials is beyond any doubt.

VII. ANALYTICAL ANALYSIS OF SECONDARY INSTABILITIES

We present our analytical understanding of secondary instabilities. The Eckhaus instability can be analyzed in the context of phase dynamics [21], and we shall not discuss it here. The parity-breaking and period-halving bifurcations are analyzed close to the codimension-two bifurcation, where the first and second harmonics are both quasineutral. This will be sufficient to understand the basic ingredients. The analysis of the vacillating-breathing mode is based on an analogy with the problem of quasi-free-electrons in a crystal.

A. Parity-breaking and period-halving bifurcations

This analysis is based on a model of two-mode interactions. This type of treatment is analogous to the one first presented by Malomed and Tribelsky [22]. Since our equations contain new terms, it is worthwhile to repeat briefly the analysis. Close to the primary bifurcation (i.e., the bifurcation from the planar to the cellular state) only the first harmonic is active. As l_T^{-1} decreases, the second harmonic becomes more and more important. Figure 14 shows the region where the first and second harmonics are both unstable (the hatched region), and the point of codimension two where they simultaneously bifurcate. Our analysis makes sense if the distance from the codimension-two point is small enough, and we shall see below that the conclusions we are going to draw are qualitatively accurate even far away from the codimension-two point.

We restrict ourselves, without loss of generality, to the liquid-crystal system. The starting point is to expand $\zeta(X,T)$ in Eq. (4.1) in Fourier series,

$$\zeta(X,T)=A_0(T)+\sum_{n=1}^{\infty}[A_n(T)e^{iqnX}+\text{c.c.}]\ . \tag{7.1}$$

Inserting this expression into Eq. (4.1), we obtain a general equation for A_n:

$$\begin{aligned} L(nq)A_n(t) &= \sum_m \{b(n-m,m)q^2 A_{n-m}\dot{A}_m \\ &\quad + c(n-m,m)q^4 A_{n-m}A_m\} \\ &\quad + \sum_{m,p}\{d(n-m-p,m,p)q^4 A_{n-m-p}A_m A_p\}\ , \end{aligned} \tag{7.2}$$

with

$$L(q)=\frac{d^2}{dt^2}+4q^2\frac{d}{dt}+(3q^4-8q^2+8l_t^{-1})\ . \tag{7.3}$$

b, c, and d are polynomials. Close to a critical point the amplitude scales as the square root with the distance from the threshold. This means that the cubic term balances the linear one, and that therefore our expansion should be made up to the third order in amplitude. We are interested in a regime where the first and second harmonics are competitive, while higher harmonics are damped and therefore slaved to these others. We may thus naively be tempted to write Eq. (7.2) for $n=1$ and 2

up to third order, where one would keep only terms containing A_1 and A_2. This is, however, not legitimate. Indeed, although higher harmonics are damped they will react on the first two harmonics and thus renormalize the coefficients of the governing equations. Indeed, it can easily be seen from (7.2) that in the equation for A_1 we have terms like $A_2^* A_3$ (the form of this term is in fact a consequence of translational invariance). On the other hand, the slaving of A_3 results in terms like $A_3 \sim A_1 A_2$ (here again translational invariance may be invoked), so that $A_2^* A_3 \sim \|A_2\|^2 A_1$, a term which should be retained. A similar reasoning holds for the equation of A_2, where quadratic terms containing A_4 must be retained. Having taken care of these points, which are necessary to have a consistent expansion, we are in a position to write the coupled equations. They take the form

$$\begin{aligned} L(q)A_1 = {} & \alpha_1 A_1^* A_2 + \beta_1 A_1 |A_1|^2 + \gamma_1 A_1 |A_2|^2 \\ & + \delta_1 A_1^* \dot{A}_2 + \lambda_1 A_1 A_2 \dot{A}_2^* \\ & + \mu_1 A_1 \dot{A}_2 A_2^* + \nu_1 \dot{A}_1 |A_2|^2 \\ & + \rho_1 A_1 |\dot{A}_2|^2 + \sigma_1 \dot{A}_1 A_2 \dot{A}_2^* , \end{aligned} \tag{7.4}$$

$$\begin{aligned} L(2q)A_2 = {} & \alpha_2 A_1^2 + \beta_2 A_2 |A_2|^2 + \gamma_2 A_2 |A_1|^2 + \delta_2 A_1 \dot{A}_1 \\ & + \lambda_2 A_2^2 \dot{A}_2^* + \mu_2 \dot{A}_2 |A_2|^2 + \nu_2 \dot{A}_2 |A_1|^2 \\ & + \xi_2 A_1 \dot{A}_1^* A_2 + o_2 \dot{A}_1 A_1^* A_2 \\ & + \rho_2 A_2 |\dot{A}_1|^2 + \sigma_2 A_1 \dot{A}_1^* \dot{A}_2 . \end{aligned} \tag{7.5}$$

The coefficients appearing in Eqs. (7.4) and (7.5) are related to the control parameter l_T^{-1} and to the wave number q, and are listed in Appendix A. We will find it convenient to introduce a phase and an amplitude $A_1 = a_1 e^{i\phi_1}$ and $A_2 = a_2 e^{i\phi_2}$. We can in principle analyze the full equations. However, we shall first simplify them. Indeed, if the distance from the codimension-two point is small enough, this means that the growth rates $\Omega(q)$ and $\Omega(2q)$ are small. Therefore terms like $\ddot{A}_1$ are small as compared to $\dot{A}_1$. Similarly, since $A_1^* \dot{A}_2 \sim \Omega A_1^* A_2$, and Ω scales as the square of an amplitude, we shall drop these terms. In this context, the equations for the phase and amplitudes simplify greatly. The result is

$$4q^2 \dot{a}_1 = \Omega(q) a_1 + \alpha_1 a_1 a_2 \cos(\chi) + \beta_1 a_1^3 + \gamma_1 a_1 a_2^2 , \tag{7.6}$$

$$4q^2 \dot{\phi}_1 = -\alpha_1 a_1 a_2 \sin(\chi) , \tag{7.7}$$

$$16q^2 \dot{a}_2 = \Omega(2q) a_2 + \alpha_2 a_1^2 \cos(\chi) + \beta_2 a_2^3 + \gamma_2 a_1^2 a_2 , \tag{7.8}$$

$$16q^2 a_2 \dot{\phi}_2 = \alpha_2 a_1^2 \sin(\chi) , \tag{7.9}$$

where $\chi = 2\phi_1 - \phi_2$. A simple manipulation of (7.7) and (7.9) yields an equation for χ:

$$\dot{\chi} = -\frac{\alpha_1}{2q^2 a_2} \left[a_2^2 + \frac{\alpha_2}{8\alpha_1 a_1^2} \right] \sin(\chi) . \tag{7.10}$$

It is seen that if (a_1, a_2, χ) are known, then ϕ_1 and ϕ_2 will also be known. In other words, the number of degrees of freedom is three (as long as the second temporal derivatives remain small). This follows from translational invariance since one phase is arbitrary.

B. Pure and mixed modes

We first characterize the steady-state solutions of Eqs. (7.11) and (7.9). The steady version takes the form

$$\Omega(q) a_1 \pm \alpha_1 a_1 a_2 + \beta_1 a_1^3 + \gamma_1 a_1 a_2^2 = 0 , \tag{7.11}$$

$$\Omega(2q) a_2 \pm \alpha_2 a_1^2 + \beta_2 a_2^3 + \gamma_2 a_1^2 a_2 = 0 , \tag{7.12}$$

$$\sin(\chi) = 0 . \tag{7.13}$$

The plus sign corresponds to $\chi = 0$, and the minus to $\chi = \pi$. This set admits two types of solutions.

(i) Pure mode solutions P^+ and P^-. This corresponds to the case where $a_1 = 0$, and

$$a_2^2 = -\frac{\Omega(2q)}{\beta_2} . \tag{7.14}$$

This solution exists only if the right-hand side of Eq. (7.14) is positive. Figure 15 shows this solution for a given value of l_T^{-1}. Note that the modes P^+ ($\chi = \pi$) and P^- ($\chi = 0$) are identical.

(ii) Mixed mode solutions M^+ and M^-. This solution corresponds to the situation where $a_1 \neq 0$. Contrary to the previous case, we should distinguish here between the two cases $\chi = \pi$ (M^+) and $\chi = 0$ (M^-). This solution is characterized by

$$\alpha a_2^3 + \beta a_2^2 + \gamma a_2 + \delta = 0 , \tag{7.15}$$

where

$$\alpha = \beta_1 \beta_2 - \gamma_1 \gamma_2 , \quad \beta = \mp(\alpha_1 \gamma_2 + \alpha_2 \gamma_1) , \tag{7.16}$$

$$\gamma = \Omega(2q)\beta_1 - \alpha_1 \alpha_2 - \Omega(q)\gamma_2 , \quad \delta = \mp \Omega(q) \alpha_2 , \tag{7.17}$$

where the upper and lower signs refer to $\chi = 0$ and π, respectively. The value of a_1 can be obtained from (7.11). Figure 15 shows the branches M^+ and M^-. One sees there that at large enough q there is only the M^+ branch.

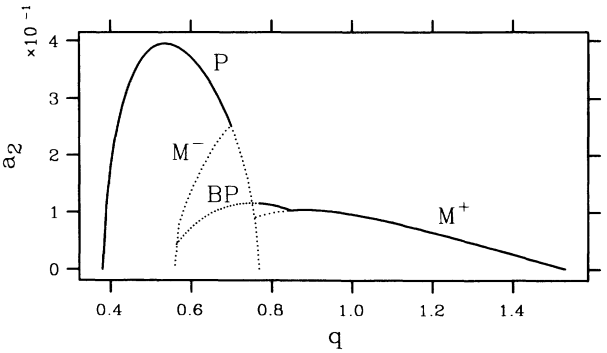

FIG. 15. The evolution of the mixed mode toward a series of instabilities (see text) in the $q - a_2$ plane for fixed l_T^{-1}. Solid lines correspond to stable states (within the two-mode approximation), dotted lines to unstable ones. Note that the BP mode is stable close to the bifurcation point in this approximation, while it is unstable there in reality.

By decreasing q the second harmonic becomes competitive. The M^+ solution ceases to exist, while the pure mode branch bifurcates. This is the period-halving bifurcation. Note that the M^+ branch corresponds to the situation where the second harmonic acts against the first one, while for M^- the second harmonic reinforces the first one.

C. Parity breaking

In the two-mode interaction picture, the front profile can be written as

$$\zeta=2a_1\cos(qX+\phi_1)+2a_2\cos(\chi)\cos[2(qX+\phi_1)] +2a_2\sin(\chi)\sin[2(qX+\phi_1)] . \tag{7.18}$$

One sees thus that a nonzero value of χ induces an antisymmetric component in the front profile. We can think of this quantity as an order parameter for parity breaking. The question now is whether Eq. (7.13) possesses a nontrivial fixed point. This occurs if the term multiplying $\sin(\chi)$ vanishes for a particular value of $\chi\neq 0$. This happens for

$$a_2^2=-\frac{\alpha_2}{8\alpha_1}a_1^2 . \tag{7.19}$$

A necessary condition is that $\alpha_1\alpha_2<0$. This is clearly the case (see the definition of the coefficients in Appendix A). The amplitudes a_1 and a_2 are functions of χ [see Eqs. (7.11) and (7.12)], so that Eq. (7.19) is an implicit equation for the unknown χ. It is a simple matter to obtain from the set (7.11) and (7.12) a closed expression for a_2 (and a_1), which upon substitution in (7.19) provides a closed expression for the order parameter. The result is

$$a_2^2=[\alpha_1\Omega(2q)-c\alpha_2\Omega(q)]/\Delta , \tag{7.20}$$

$$\cos(\chi)=[(c\beta_1+\gamma_1)\Omega(2q)-(\beta_2+c\gamma_2)\Omega(q)]/(a_2\Delta) , \tag{7.21}$$

where we have introduced the abbreviations

$$c=-\frac{\alpha_2}{8\alpha_1} , \quad \Delta=c\alpha_2(c\beta_1+\gamma_1)-\alpha_1(\beta_2+c\gamma_2) . \tag{7.22}$$

The existence of the broken-parity (BP) state is subject to the conditions $a_2^2>0$ and $\|\cos(\chi)\|<1$. Figure 15 shows the BP branch. Note that this mode branches off the M^+ one. It can also be checked that at this point the M^+ mode loses its stability. In summary the PB bifurcation results from the loss of stability of the mixed mode and occurs slightly before the period-halving bifurcation.

D. The VB instability

As described in Sec. V the model equation supports a VB instability. In this section we develop an analytical analysis which allows to shed light on this phenomenon. This analysis is inspired by the problem of a quasifree electron in a crystal. It will be recognized below that although our analysis will be concerned with Eq. (4.1), the spirit will perfectly operate in more general situations.

Let ζ_{0q} designate the steady-state solution parametrized by the wave vector q, and denote by $\zeta_1(X,T)$ an arbitrary but small deviation about the steady solution. For the sake of simplicity we concentrate on the situation where mass diffusion is symmetric, and where the miscibility gap is constant (i.e., $\nu=1$ and $k=1$). Linearizing Eq. (4.1), we obtain

$$\zeta_{1TT}-4\zeta_{1XXT}+3\zeta_{1XXXX}+8\zeta_{1XX}+8l_T^{-1}\zeta_1=4\zeta_{0qx}\zeta_{1XT}+2\zeta_{0qXX}\zeta_{1T}-12\zeta_{0qXX}\zeta_{1XX}-6\zeta_{0qX}^2\zeta_{1XX} -8\zeta_{0qX}\zeta_{1XXX}-8\zeta_{0qXXX}\zeta_{1X}-12\zeta_{0qXX}\zeta_{0qX}\zeta_{1X} . \tag{7.23}$$

This is a linear equation with periodic coefficients due to the periodicity of ζ_{0q}. Thus it is analogous to the Schrödinger equation with a periodic potential, familiar from the problem of an electron in a crystal. As is the case with the Schrödinger equation, there is in general no exact solution. However, if our wish is to understand the basic ingredient of some features, a perturbation theory may be sufficient. For example, in order to understand the appearance of energy-band structures, it is instructive to make use of a quasi-free-electron approximation. In the present case the potential analogs are the derivatives of ζ_0. Since the wave number of interest is of order one, the amplitude of ζ_0 is (approximately) the amplitude of the potential. Recall that the cellular structure takes place at a value $l_T^{-1}=l_{Tc}^{-1}=\frac{2}{3}$, and at that point the amplitude of deformation increases continuously from zero. The full numerical analysis has shown that the VB instability takes place in a regime where only the first harmonic is active. Therefore it is reasonable to assume that the steady solution is composed of the first harmonic only. On the other hand a simple analysis of the bifurcation equations treated in Sec. VII C shows that $a_1\sim 0.2-0.3$, close enough to the birth of the VB mode. Since the leading coefficient not multiplying ζ_0 in Eq. (7.23) is of order unity, it is legitimate to treat, ζ_0 as a perturbation in Eq. (7.23), on a first level.

Since Eq. (7.23) is autonomous with respect to time, the eigenfunction $\zeta_1(X,T)=e^{\omega T}\hat{\zeta}(X)$, where ω is the eigenvalue (it plays a similar role to the energy in quantum mechanics). The form of eigenfunction ζ_1 follows from the Floquet-Bloch theorem, and we shall write it as

$$\hat{\zeta}(X)=\cdots+b_{-1}e^{i(Q-q)X}+b_0e^{iQX}+b_1e^{i(Q+q)X}+\cdots . \tag{7.24}$$

We can think of b_0 as the amplitude of the incident wave

function, b_{-1} that of the reflected one (the analog of the Bragg reflection), and b_1 that of the transmitted wave function. In the bare problem ($\zeta_0=0$) we can determine a zeroth-order energy given by

$$\omega_n=-2(Q+nq)^2+\{(Q+nq)^4+8(Q+nq)^2-8l_T^{-1}\}^{1/2}, \tag{7.25}$$

where n is integer, and where we omit the other solution with a minus sign in front of the square root, since it is a stable Mullins-Sekerka branch. If we consider only the first Brillouin zone (i.e., $0<Q/q<1$) we distinguish there between three intersections of branches ω_n, one at $Q=0$, a second one at $Q/q=\frac{1}{2}$, and a third one with Q/q close to $\frac{1}{2}$. In the representation we have chosen, the three intersections are represented by the equations $\omega_1=\omega_{-1}$, $\omega_0=\omega_{-1}$, and $\omega_0=\omega_1$, respectively. In the problem of a quasifree electron, only the intersection between the spectrum of the incident wave and the reflected one is crucial (a part of the reason is that the other intersections are associated with highly excited states, while this is not the case here because of the topology of the bare energy which makes the intersection between ω_0 and ω_{-1}, and ω_0 and ω_1, both close to the Q axis, and therefore both potentially dangerous).

It is clear that the most relevant contribution of the spectrum where the waves are coupled [via the terms proportional to ζ_0 in Eq. (7.23)] comes from the resonance due to the energy degeneracy. Let us treat each resonance separately.

1. The Bragg-like resonance

The standard resonance is the one which occurs for the problem of an electron in a crystal. That is, it corresponds to the resonance between the incident wave (whose amplitude is b_0) and the reflected one (whose amplitude is b_{-1}; it is the analog of the Bragg reflection). Close to the intersection point, the total wave function is a linear combination of the two functions:

$$\hat{\zeta}(X)=b_{-1}e^{i(Q-q)X}+b_0e^{iQX}. \tag{7.26}$$

Inserting this into Eq. (7.23), we obtain a set of two linear and homogeneous equations for the coefficients b_{-1} and b_0. The condition for the existence of a nontrivial solution yields the dispersion relation. The detailed calculation is given in Appendix B. At the intersection point $Q/q=\frac{1}{2}$, the dispersion relation provides, to leading order in the amplitude a_1,

$$\omega=\omega_0\pm\frac{|a_1|}{\{(q/2)^4+8(q/2)^2-8l_T^{-1}\}^{1/2}}q^4. \tag{7.27}$$

Note that the radicand of the denominator in Eq. (7.27) is positive for growing states [$Re(\omega_0)>0$]. This result is very similar to the one encountered for an electron in a crystal: the effect of the underlying periodic solution results in the creation of an energy gap. The creation of an energy gap simply shows that extended solutions are those which correspond to ω given by (7.27).

The most interesting result, which has no analog in the problem of an electron in a crystal, is the one which arises in the analysis below.

2. The VB resonance

In quantum mechanics only resonances with energy-gap creations are permissible. The deep reason is that the energy is an observable, and consequently the associated operator, the Hamiltonian, is self-adjoint. There is no such restriction in the problem we are studying, and operators do not necessarily have to be self-adjoint. In particular, the linear operator [Eq. (7.23)] under consideration is obviously not self-adjoint.

There is in the present case *a* the creation of a *wave-vector gap* instead of an energy gap [23]. A corollary of this is that energy becomes *complex*. This feature is the reason for the birth of the VB mode. The calculation is similar to the one presented above. The only difference now is to replace b_{-1} by b_1 (and the bare spectrum accordingly). The calculation presented in Appendix B shows that

$$\omega=\omega_0(Q)\pm 2i|a_1|\frac{|\{q^8-[q(q+2Q)\omega_0(Q)+(Q+q)^4-Q^4]^2\}|^{1/2}}{|[\omega_0(Q)-\sigma_0(Q)][\omega_0(Q)-\sigma_0(Q+q)]|^{1/2}}. \tag{7.28}$$

This result shows that the coupling of the two branches $Q+q$ and Q leads to oscillatory states. This result has no analog in quantum mechanics, where no complex eigenvalues are permissible. This analysis shows the origin of VB modes.

At this stage we have not yet found which value of Q is the most dangerous. This is what we would like to accomplish now. For that purpose we have analyzed Eq. (7.28) in the parameter space (l_T^{-1},q) and looked for the boundary where $\mathrm{Re}(\omega)$ crosses zero. Figure 16 show this boundary below which $\mathrm{Re}(\omega)>0$ and along which $\mathrm{Im}(\omega)\neq 0$. The solid line represents the case where the most dangerous value of Q is 0.5 (the true VB state), and where there is a good agreement with the full calculation presented in Sec. V D. In particular, for $l_T^{-1}=0.3$ and $q=0.9$, here we find $\mathrm{Im}(\omega)\simeq 0.86$, while in the full calculation $\mathrm{Im}(\omega)\simeq 0.9$. The dotted lines represent the case where Q is irrational. In the full calculation presented in Sec. V D we did not encounter the latter situation. This is not surprising. Indeed, our analytic calculation is not expected to be accurate (i) when we approach the line where the second harmonic becomes neutral, and it

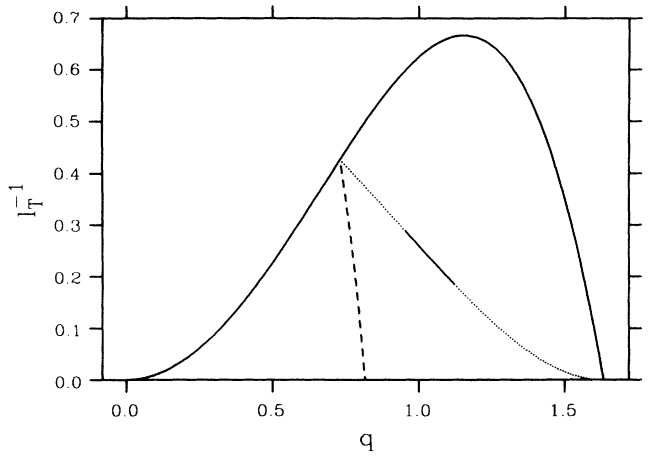

FIG. 16. The solid line: the neutral curve. The combined dotted and solid curve represents the line, below which a VB mode appears. The dotted parts represent the case where the instability wave number Q is "irrationally" related to q (see text).

would be necessary to include it; and (ii) when we consider small values of l_T^{-1}, and $|a_1|$ becomes larger and larger, so that the validity of perturbation analysis breaks down.

VIII. BEYOND SECONDARY INSTABILITIES

The secondary instabilities are the beginning of a route toward the formation of more complex and richer patterns. The most important feature is that the VB mode is itself susceptible to parity breaking, before the dynamics enter a chaotic regime. On the other hand, the BP mode may undergo an oscillatory instability, depending on the path in parameter space. For decreasing wave number at a constant value of l_T^{-1}, this leads to a permanent hopping of the pattern between the q and $2q$ modes, which is a prelude to another type of chaos [24]. These transitions to chaos are a subject by themselves, which is presented in the companion paper. Below we discuss some other dynamic features.

A. Anomalous cells

The parity-breaking bifurcation is a pitchfork bifurcation: the right- and left-traveling states are both solutions to the growth equations. Due to this degeneracy, we can construct other solutions, as in domain-wall structures. One of the solutions is that where the front consists of alternating leftlike and rightlike cells. There is *a priori* no reason that the two types of cells have the same lateral width. We have not yet addressed such a general question. The case we have dealt with so far is the one where the pattern consists of pairs of asymmetric cells with one being the mirror image of its two neighbors. In this case the pattern does not drift. We refer to this growth mode as the *anomalous state.* We have shown the existence of this state in eutectic systems [25], both numerically and analytically.

In the present model, both steady-state and dynamical

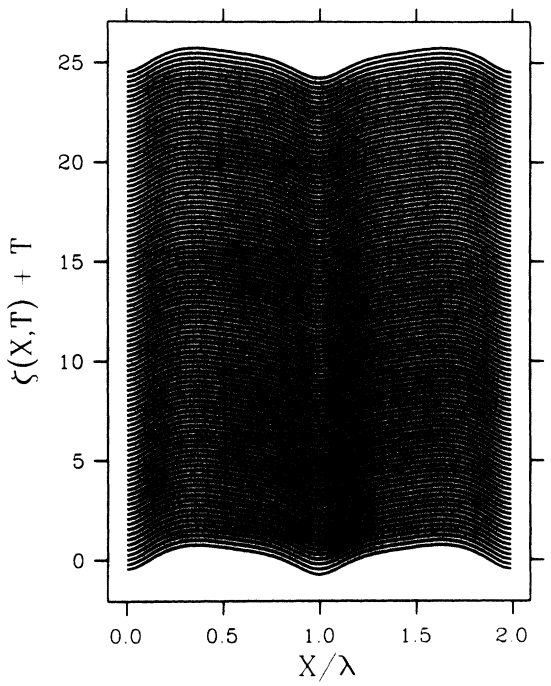

FIG. 17. Anomalous states. An example for the symmetric model $-l_T^{-1}=0.28$, $q=0.8$, and $\nu=1.0$.

considerations reveal the existence of such a solution (Fig. 17) in both symmetric and one-sided limits. This solution typically exists in a region of parameter space, where the BP solution is also present. This type of solution was observed in many systems, but the most spectacular observation is that of Jamgotchian *et al.* [26] during directional growth of succinonitrile.

B. Long-wavelength instabilities of the BP state

In the context of the phenomenological model of Coullet, Goldstein, and Gunaratne [9], Fauve, Douady, and Thual [27] pointed out that the broken-parity state suffers a long-wavelength oscillatory instability near its bifurcation point. It is therefore natural to ask whether such an instability is present within a microscopic model, and if so, what would be the subsequent dynamics. To study this question we have performed a full linear stability analysis on Eq. (4.1), after having made the transformation into the moving frame. The strategy is then similar to that used in Sec. V: we first investigate a traveling solution characterized by its drift velocity, and then use a systematic Floquet-Bloch theory. We find that, at and above their birth point (from the initially symmetric state), the broken-parity states indeed suffer the above-mentioned instability. We have compared our results, concerning the dependence of the real and imaginary parts on the wave number Q, with those following from the phenomenology presented by Fauve, Douady, and Thual [28]. From amplitude equations, for the growth rate they obtain

$$\omega^2+(2v^2-iQgv+bQ^2)\omega-iQfv+aQ^2=0\ . \qquad (8.1)$$

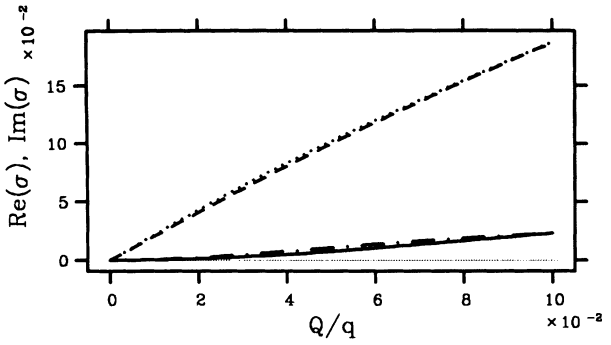

FIG. 18. Comparison of the real and imaginary parts of the eigenvalues for the stability of the BP state. Solid and dashed lines: real and imaginary parts obtained in the full calculation ($l_T^{-1}=0.28$, $q=0.8$, and drift velocity $v=0.388$); dash-dotted and dotted lines: the same for the phenomenological model [Eq. (8.1)], where the parameters were taken to be $v=0.388$, $a=2.0$, $b=g=1.0$, and $f=1.7$.

Herein a, b, f, and g are phenomenological coefficients, and a and b are assumed to be positive. v is the lateral drift velocity. The most important coefficient is f, which multiplies the gradient of the phase of the pattern in the amplitude equations and destabilizes the drifting pattern independent of its sign, for not too large drift velocity. In Fig. 18, we compare the solution to Eq. (8.1) with that of our exact stability analysis of a BP mode not too far from its bifurcation point. We obtain good agreement between the two treatments for model parameters $a-g$ on the order of 1 (see the figure for details).

An important consequence of this instability is that the BP state is probably not observable as an extended state (except in eutectics [29,30], where the slowness of phase diffusion inhibits the instability). It should undergo a fragmentation process. The different scenarios that we have encountered cannot be described here, but we have selected some typical behaviors, in the present paper and its companion. For $q=0.85$ and $l_T^{-1}=0.26$ (with $\nu=1$ and $k=1$), the evolution of the initially extended BP state is shown in Fig. 19 (the computational box contains initially ten cells). After a complex mechanism involving tip splitting and cell creation, an oscillatory structure emerges, with an average wave number $q=1.02$, that behaves relatively regularly (there is some irregularity: every once in a while sources appear, from which two localized waves are emitted in opposite directions). Longer simulations show that this pattern retains it character. A noticeable point is the presence of a global drift of the envelope of the pattern, while the single cells remain roughly stationary. There are two light bands in the pattern of Fig. 19, consisting of features which bear some resemblance to the solitary modes discovered in liquid-crystal experiments by Simon, Bechhoefer, and Libchaber [3]. An even more regular structure, where these features are more strongly pronounced, can be found by starting from $q=0.9$ (corresponding to an unstable *symmetric* state) and ending at $q=1.08$. For details, see Ref. [19].

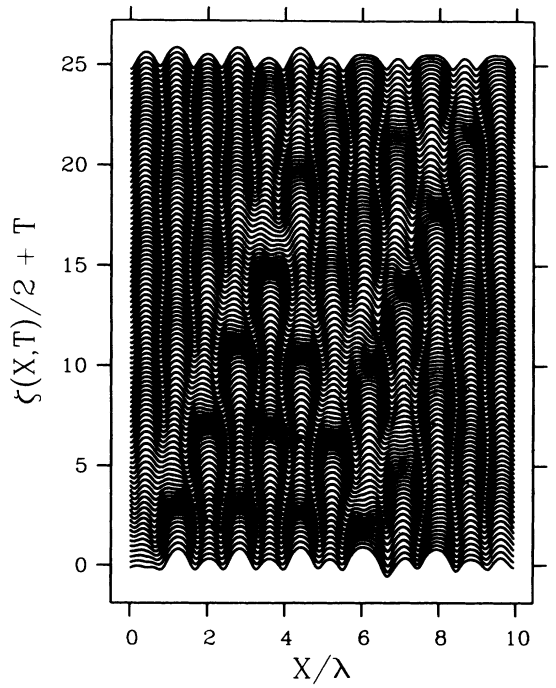

FIG. 19. Evolution of an initially asymmetric state revealing a long-wave-length instability. Here we represent only the permanent regime, where, by following the cells that almost split, we can see two light bands along which we can recognize features which bear resemblance to the solitarylike mode observed in experiments on liquid crystals [3]. Here the amplitude of the cells has been reduced by a factor 0.5 for a clearer picture.

IX. CONCLUSION

This paper has dealt with a number of features, most of them pertaining to secondary instabilities of a crystallization front. The focus was on the large speed regime (by large we mean a diffusion length comparable to the chemical capillary length) which is more tractable than the usual full boundary integral equation. This has allowed us to capture in an easy way (and therefore enlightening) the essential physical concepts of the various instabilities. We did not notice any relevance of the values of the material parameters to any one of the features investigated here. We can thus ascertain the general relevance of the present study to a wide range of systems, ranging from metals to liquid crystals.

It is fascinating to see that a simple system, such as a one-dimensional front whose motion is limited by diffusion, exhibits a myriad of behaviors. We believe, however, that this paper and its companion are far from exhausting all the features.

Most of the instabilities reported here have been observed on a variety of fronts [3–6], as well as in many hydrodynamical systems [7,8]. There is no hint, however, that the equation on which the present study was performed should be generic in the sense that it can apply to the diverse list of physical systems. A recent study [31] has shown that the stabilized Kuramoto-Sivashinsky (SKS) equation is generic. It has been shown that this equation exhibits all the features reported here, plus oth-

ers which are not exhibited by the present equation [31]. The SKS equation, which is simpler than the one encountered in directional growth, reinforces our belief that the variety of patterns in physical and chemical systems, and so on, which at first sight seem extremely diverse, are most likely a disguised form of only a few prototypes. It will be an important task for future investigations to recognize, at least in the hydrodynamic limit, the relevant nonlinearities in the equation on which the present study was performed, and possibly to elucidate the question of whether this equation enters a universality class or not.

ACKNOWLEDGMENTS

K. K., C. M., and A. V. benefited from financial support under NATO Grant No. CRG.920541. Part of this work was accomplished while C. M. was visiting the Forschungszentrum Jülich. C. M. would like to express his gratitude for the hospitality and financial support. The Laboratoire de Spectrométrie Physique is "Unite Recherche 08 au CNRS."

APPENDIX A: LIST OF THE COEFFICIENTS APPEARING IN THE COUPLED EQUATIONS

In this appendix, we give expressions for the coefficients involved in the coupled equations (7.4) and (7.5). They are given by

$$\alpha_1=32q^2\ ,\quad \alpha_2=-14q^4\ , \tag{A1}$$

$$\beta_1=6q^4\ ,\quad \beta_2=96q^4+\frac{224\times 512q^8}{\Omega(4q)}\ , \tag{A2}$$

$$\gamma_1=48q^4+\frac{128\times 192q^8}{\Omega(3q)}\ ,\quad \gamma_2=48q^4+\frac{128\times 132q^8}{\Omega(3q)}\ , \tag{A3}$$

$$\delta_1=6q^2\ ,\quad \delta_2=-6q^2\ , \tag{A4}$$

$$\lambda_1=\frac{6\times 128q^6}{\Omega(3q)}\ ,\quad \lambda_2=0\ , \tag{A5}$$

$$\mu_1=\frac{10\times 192q^6}{\Omega(3q)}\ ,\quad \mu_2=\frac{24\times 512q^6}{\Omega(4q)}\ , \tag{A6}$$

$$\nu_1=\frac{16\times 192q^6}{\Omega(3q)}\ ,\quad \nu_2=\frac{10\times 132q^6}{\Omega(3q)}\ , \tag{A7}$$

$$\rho_1=\frac{6\times 10q^4}{\Omega(3q)}\ ,\quad \rho_2=-\frac{6\times 16q^4}{\Omega(3q)}\ , \tag{A8}$$

$$\sigma_1=\frac{6\times 16q^4}{\Omega(3q)}\ ,\quad \sigma_2=-\frac{6\times 10q^4}{\Omega(3q)}\ , \tag{A9}$$

and

$$o_2=-\frac{6\times 128q^6}{\Omega(3q)}\ ,\quad \xi_2=-\frac{16\times 132q^6}{\Omega(3q)}\ . \tag{A10}$$

APPENDIX B: BRAGG-LIKE AND VB RESONANCE

In this appendix, we present detailed calculation of the eigenvalues for the Bragg-like and VB resonances.

Let us first examine the Bragg-like resonance, which corresponds to the situation where $\omega_0(Q)=\omega_{-1}(Q)[\equiv\omega_0(Q-q)]$. The eigenstate close to this intersection is a superposition of two wave functions:

$$\hat{\xi}(x)=b_{-1}e^{i(Q-q)x}+b_0e^{iQx}\ . \tag{B1}$$

Inserting this into (4.1), we obtain the following set of equations for b_{-1} and b_0:

$$-\{[-4q(Q-q)-2q^2]\omega+[-12q^2(Q-q)^2-8q(Q-q)^3-8q^3(Q-q)]\}a_1b_{-1}+\{\omega^2+4Q^2\omega-[-3Q^4+8Q^2-8l_T^{-1}]\}b_0=0\ , \tag{B2}$$

$$\{\omega^2+4(Q-q)^2\omega-[-3(Q-q)^4+8(Q-q)^2-8l_T^{-1}]\}b_{-1}-\{[4qQ-2q^2]\omega+[-12q^2Q^2+8qQ^3+8q^3Q]\}a_{-1}b_0=0\ . \tag{B3}$$

Note that we have kept only the leading nonlinear terms in the amplitude $|a_1|$. Requiring the determinant of this system to be identically zero, we obtain the equation for the eigenvalues ω, which can be written as follows:

$$\begin{aligned}[\omega-\omega_0(Q)][\omega-\omega_0(Q-q)][\omega-\sigma_0(Q)][\omega-\sigma_0(Q-q)]&\\ =4|a_1|^2[6q^2(Q-q)^2+4q(Q-q)^3+4q^3(Q-q)+q(2Q-q)\omega][6q^2Q^2-4qQ^3-4q^3Q-q(2Q-q)\omega]&\\ =4|a_1|^2[Q^4-(Q-q)^4-q^4+q(2Q-q)\omega]\times[(Q-q)^4-Q^4-q^4-q(2Q-q)\omega]&\\ =4|a_1|^2\{q^8-[q(q-2Q)\omega+(Q-q)^4-Q^4]^2\}\ ,&\end{aligned} \tag{B4}$$

where we have set

$$\sigma_0(Q)=-2Q^2-[Q^4+8Q^2-8l_T^{-1}]^{1/2}\ . \tag{B5}$$

At this stage, we have not yet used that at the intersection point we have $Q=q/2$. Doing so, we obtain

$$\omega=\omega_0(Q)+\delta \ , \tag{B6}$$

where δ is of order of $|a_1|$. A simple algebraic manipulation yields

$$\delta^2=\frac{4|a_1|^2\{q^8-[q(q-2Q)\omega_0(Q)+(Q-q)^4-Q^4]^2\}}{[\omega_0(Q)-\sigma_0(Q)][\omega_0(Q)-\sigma_0(Q-q)]} \ . \tag{B7}$$

At this stage, we have not yet used that at the intersection point we have $Q=q/2$. Doing so, we obtain

$$\delta^2=\frac{4|a_1|^2q^8}{|\omega_0(q/2)-\sigma_0(q/2)|^2}=\frac{|a_1|^2q^8}{|(q/2)^4+8(q/2)^2-8l_T^{-1}|} \ . \tag{B8}$$

We can now write the final expression of the eigenvalue ω as

$$\omega=\omega_0(q/2)\pm\frac{|a_1|q^4}{|(q/2)^4+8(q/2)^2-8l_T^{-1}|^{1/2}} \ . \tag{B9}$$

This result means that the resonant coupling between the incident wave Q and the reflected one $Q-q$ results in the creation of an energy gap, similar to the energy gap in solid-state physics.

Let us now deal with the VB mode which corresponds to the situation where the incident wave function couples to the transmitted one (i.e., where $\omega_0(Q)=\omega_1(Q)[\equiv\omega_0(Q+q)]$). In this case, the eigenmode takes the form

$$\hat{\xi}(x)=b_0e^{iQx}+b_1e^{i(Q+q)x} \ , \tag{B10}$$

which leads to the following system:

$$\{[4q(Q+q)-2q^2]\omega+[-12q^2(Q+q)^2+8q(Q+q)^3+8q^3(Q+q)]\}a_{-1}b_1 \\ -\{\omega^2+4Q^2\omega-[-3Q^4+8Q^2-8l_T^{-1}]\}b_0=0 \ , \tag{B11}$$

$$\{\omega^2+4(Q+q)^2\omega-[-3(Q+q)^4+8(Q+q)^2-8l_T^{-1}]\}b_1+\{[4qQ+2q^2]\omega+[12q^2Q^2+8qQ^3+8q^3Q]\}a_1b_0=0 \ . \tag{B12}$$

As previously, only the leading-order terms in the amplitude $|a_1|$ have been retained. The solubility condition of this system give us the equation for the eigenvalues:

$$[\omega-\omega_0(Q)][\omega-\omega_0(Q+q)][\omega-\sigma_0(Q)][\omega-\sigma_0(Q+q)]=4|a_1|^2\{q^8-[q(q+2Q)\omega+(Q+q)^4-Q^4]^2\} \ . \tag{B13}$$

Writing

$$\omega=\omega_0(Q)+\delta \ , \tag{B14}$$

we obtain

$$\delta^2=\frac{4|a_1|^2\{q^8-[q(q+2Q)\omega_0(Q)+(Q+q)^4-Q^4]^2\}}{[\omega_0(Q)-\sigma_0(Q)][\omega_0(Q)-\sigma_0(Q+q)]} \ . \tag{B15}$$

It is easy to check that δ^2 is negative in almost all interesting cases. Plotting the numerator as a function of q for fixed l_T^{-1} (Q is determined from q by the intersection condition), we find that for $l_T^{-1}>0.2$, δ^2 is negative whatever the value of q. For smaller l_T^{-1}, there is a small interval of q values around $q=1.5$, where δ^2 is positive. In that region we do not expect our perturbation theory to work in any case. As for the denominator, it is always positive since $\sigma_0(Q)$ is negative whatever the value of Q.

The final result can be then written as

$$\omega=\omega_0(Q)\pm 2i|a_1|\frac{|\{q^8-[q(q+2Q)\omega_0(Q)+(Q+q)^4-Q^4]^2\}|^{1/2}}{|[\omega_0(Q)-\sigma_0(Q)][\omega_0(Q)-\sigma_0(Q+q)]|^{1/2}} \ . \tag{B16}$$

One sees that now the resonance results in the appearance of a complex eigenvalue.

[1] W. W. Mullins and R. F. Sekerka, J. Appl. Phys. **325**, 444 (1964).
[2] P. Oswald, J. Bechhoefer, and A. Libchaber, Phys. Rev. Lett. **58**, 2318 (1987).
[3] A. J. Simon, J. Bechhoefer, and A. Libchaber, Phys. Rev. Lett. **63**, 2574 (1988).
[4] C. Faivre, S. de Cheveigné, C. Guthmann, and P. Kurowski, Europhys. Lett. **9**, 779 (1989).
[5] M. Rabaud, S. Michalland, and Y. Couder, Phys. Rev. Lett. **64**, 184 (1990).

[6] P. Oswald, J. Phys. (France) II **1**, 671 (1991).
[7] I. Mutabazi, H. Hegset, C. D. Andereck, and J. Wesfreid, Phys. Rev. Lett. **64**, 1729 (1990).
[8] L. Limat, P. Jenffer, B. Dagens, E. Touron, M. Fermigier, and J. E. Wesfreid, Physica D **61**, 166 (1992).
[9] P. Coullet, R. Goldstein, and G. H. Gunaratne, Phys. Rev. Lett. **63**, 2574 (1989).
[10] K. Kassner and C. Misbah, Phys. Rev. Lett. **65**, 1458 (1990); **66**, 522(E) (1991); C. Misbah and D. E. Temkin, Phys. Rev. A **46**, R4499 (1992).
[11] H. Levine and W. J. Rappel, Phys. Rev. A **42**, 7475 (1990).
[12] K. Kassner, C. Misbah, and H. Müller-Krumbhaar, Phys. Rev. Lett. **67**, 4551 (1991).
[13] P. Coullet and G. Iooss, Phys. Rev. Lett. **64**, 866 (1990).
[14] A. Karma and A. Sarkissian, Phys. Rev. Lett. **68**, 2616 (1992), and references therein.
[15] B. Caroli, C. Caroli, and B. Roulet, J. Phys. (Paris) **43**, 1767 (1982).
[16] C. Misbah (unpublished).
[17] K. Brattkus and S. H. Davis, Phys. Rev. B **38**, 11452 (1988).
[18] A. Ghazali and C. Misbah, Phys. Rev. A **46**, 5026 (1992).
[19] K. Kassner, *Pattern Formation in Diffusion-Limited Crystal Growth* [World Scientific, Singapore (in press)].
[20] K. Brattkus and C. Misbah, Phys. Rev. Lett. **64**, 1935 (1990), and references therein.
[21] A. Valance, Stage de DEA de Physique, Université Paris 7, 1991.
[22] B. A. Malomed and M. I. Tribelsky, Physica D **14**, 67 (1984); M.R. E. Proctor and C. A. Jones, J. Fluid Mech. **188**, 301 (1988); H. Levine, W. J. Rappel, and H. Riecke, Phys. Rev. A **43**, 1122 (1991).
[23] By this we mean that there is a gap in the wave numbers corresponding to real growth rates ω. Of course, ω is defined for *all* wave numbers. Alternatively, one could say that a gap is created in the imaginary part of ω (which was zero before the interaction).
[24] A. Valance, K. Kassner, and C. Misbah, Phys. Rev. Lett. **69**, 1544 (1992).
[25] K. Kassner, A. Valance, C. Misbah, and D. E. Temkin, Phys. Rev. E **48**, 1091 (1993).
[26] H. Jamgotchian, R. Trivedi, and B. Billia, Phys. Rev. E **47**, 4313 (1993).
[27] S. Fauve, S. Douady, and O. Thual, Phys. Rev. Lett. **65**, 385 (1990).
[28] S. Fauve, S. Douady, and O. Thual, J. Phys. (France) II **1**, 311 (1991).
[29] K. Kassner and C. Misbah, Phys. Rev. A **44**, 6533 (1991).
[30] G. Faivre and J. Mergy, Phys. Rev. A **45**, 7320 (1992).
[31] C. Misbah and A. Valance, Phys. Rev. E **49**, 166 (1994).

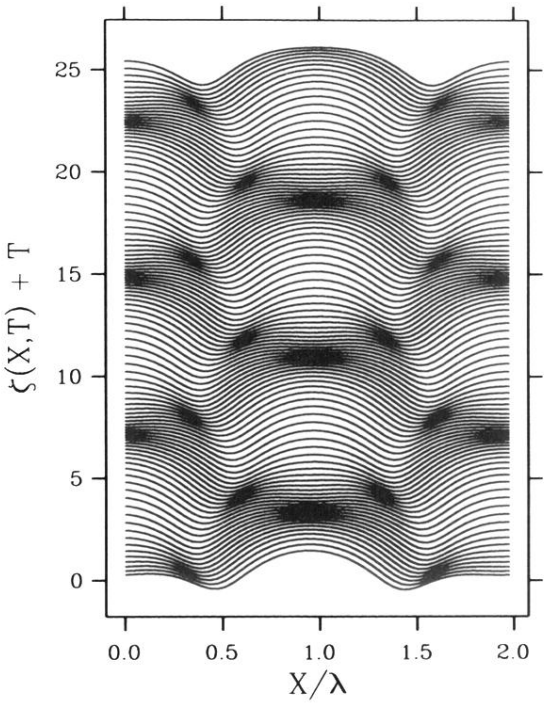

FIG. 10. The spatiotemporal portrait for the VB mode, where $l_T^{-1}=0.285$ and $q=0.9$.

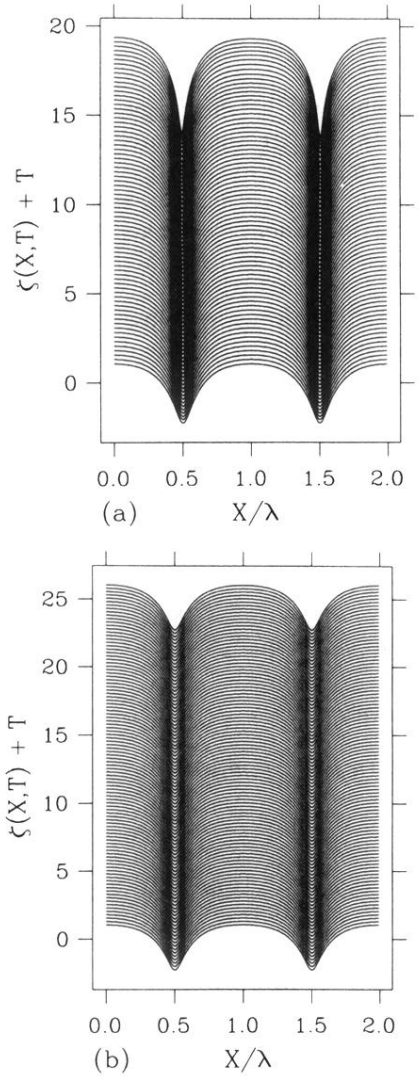

FIG. 11. A pattern showing the development of a cusp singularity (a) in the one-sided model ($\nu=0$), which is cured after allowance of a small amount of diffusion ($\nu=10^{-2}$) in the solid phase (b). Parameters: $l_T^{-1}=0.5$ and $q=1.2$.

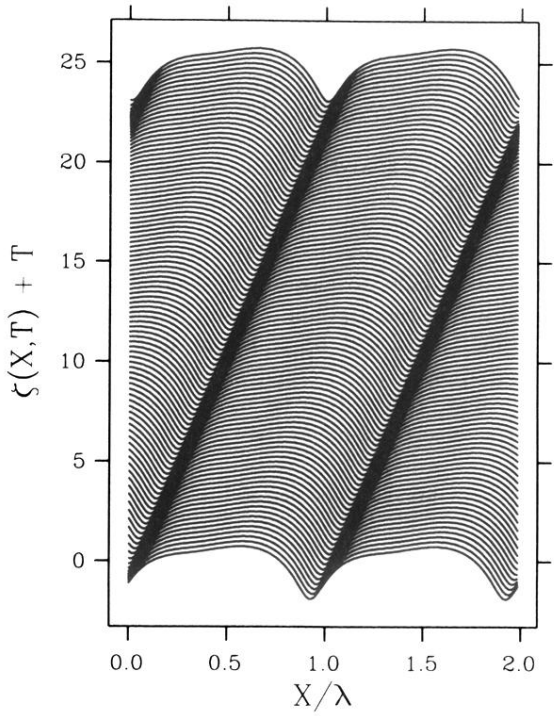

FIG. 12. The spatiotemporal portrait of a BP state in the one-sided model ($\nu=0$). Parameters: $l_T^{-1}=0.55$ and $q=1.0$.

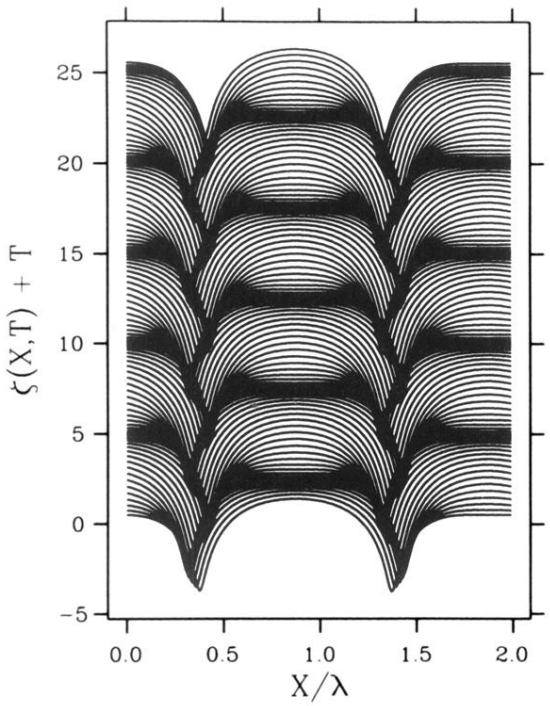

FIG. 13. The spatiotemporal portrait of the VB state in the one-sided model. Parameters: $l_T^{-1}=0.52$ and $q=1.2$.

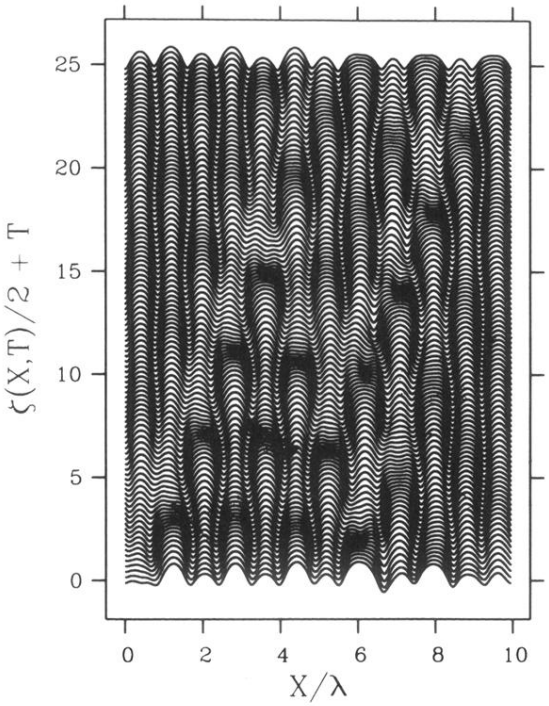

FIG. 19. Evolution of an initially asymmetric state revealing a long-wave-length instability. Here we represent only the permanent regime, where, by following the cells that almost split, we can see two light bands along which we can recognize features which bear resemblance to the solitarylike mode observed in experiments on liquid crystals [3]. Here the amplitude of the cells has been reduced by a factor 0.5 for a clearer picture.